

From head to tail: A neuromechanical model of forward locomotion in *C. elegans*

Article submitted to Philosophical Transactions of the Royal Society B. Special Issue: Connectome to behaviour: Modelling *C. elegans* at cellular resolution

Eduardo J. Izquierdo and Randall D. Beer

Cognitive Science Program, School of Informatics, Computing, and Engineering, Indiana University

Keywords:

invertebrate, locomotion, motor control, neuromechanical model, proprioception

Author for correspondence:

Eduardo J. Izquierdo
e-mail: edizquie@indiana.edu

With 302 neurons and a near complete reconstruction of the neural and muscle anatomy at the cellular level, *C. elegans* is an ideal candidate organism to study the neuromechanical basis of behavior. Yet, despite the breadth of knowledge about the neurobiology, anatomy and physics of *C. elegans*, there are still a number of unanswered questions about one of its most basic and fundamental behaviors: forward locomotion. How the rhythmic pattern is generated and propagated along the body is not yet well understood. We report on the development and analysis of a model of forward locomotion that integrates the neuroanatomy, neurophysiology and body mechanics of the worm. Our model is motivated by experimental analysis of the structure of the ventral cord circuitry and the effect of local body curvature on nearby motoneurons. We developed a neuroanatomically-grounded model of the head motoneuron circuit and the ventral nerve cord circuit. We integrated the neural model with an existing biomechanical model of the worm's body, with updated musculature and stretch receptors. Unknown parameters were evolved using an evolutionary algorithm to match the speed of the worm on agar. We performed 100 evolutionary runs and consistently found electrophysiological configurations that reproduced realistic control of forward movement. The ensemble of successful solutions reproduced key experimental observations that they were not designed to fit, including the wavelength and frequency of the propagating wave. Analysis of the ensemble revealed that head motoneurons SMD and RMD are sufficient to drive dorsoventral undulations in the head and neck and that short-range posteriorly-directed proprioceptive feedback is sufficient to propagate the wave along the rest of the body.

1 Introduction

2

2 Behavior is grounded in the interaction between an organism's brain, its body, and its
3 environment. How simple neuronal circuits interact with their muscles and mechanical bodies
4 to generate behavior is not yet well understood. With 302 neurons and a near complete
5 reconstruction of the neural and muscle anatomy at the cellular level [1], *C. elegans* is an ideal
6 candidate organism to understand the neuromechanical basis of behavior.

7 Locomotion is essential to most living organisms. Since nearly the entire behavioral repertoire
8 of *C. elegans* is expressed through movement, understanding the neuromechanical basis of
9 locomotion is especially critical as a foundation upon which analyses of all other behaviors
10 must build. *C. elegans* locomotes in an undulatory fashion, generating thrust by propagating
11 dorsoventral bends along its body. Movement is generated by body wall muscles arranged
12 in staggered pairs along four bundles [2]. The anterior-most muscles are driven by a head
13 motoneuron circuit and the rest of the muscles are driven by motoneurons in the ventral
14 nerve cord (VNC). Although the nematode is not segmented, a statistical analysis of the VNC
15 motoneurons in relation to the position of the muscles they innervate revealed a repeating neural
16 unit [3]. Interestingly, while the repeating neural units in the VNC are interconnected via a set of
17 chemical and electrical synapses, the head motoneuron circuit is largely disconnected from the
18 VNC neural units. Motoneurons in both the head and the VNC circuit have been long postulated
19 to be mechanosensitive to stretch [1, 4, 5], and evidence in support of this has been shown recently
20 for the VNC [6]. Despite all of this anatomical knowledge, how the rhythmic pattern is generated
21 and propagated along the body during forward locomotion on agar is not yet well understood.

22 A number of computational models of *C. elegans* locomotion have been proposed (see
23 reviews [7, 8, 9]). The model described in this paper differs from previous models in four
24 main ways. First, the current model of the VNC incorporates the analysis of its repeating
25 structure [3]. Second, the current model of stretch-receptor feedback takes into consideration
26 findings regarding the range and directionality of local body curvature on motoneurons [6].
27 Third, the current model integrates the head motoneuron circuit and the VNC motoneuron circuit
28 within a physical model of the body and environment, such that the forward motion of the
29 model emerges from the undulation of the head, neck, and body. Finally, all current models have
30 assumed specific mechanisms for how the rhythmic movement is generated and propagated, with
31 little systematic exploration of the possibilities.

32 Here we present a model of forward locomotion grounded in the neurobiology, anatomy, and
33 physics of the worm. The model integrates a head motoneuron circuit based on hypotheses
34 postulated in the original "Mind of the Worm" paper [1] with a model of a repeating
35 neural unit in the VNC based on a statistical analysis of the available connectome data [3].
36 Motoneurons innervate an anatomically grounded model of the muscles. Stretch receptors are
37 modeled to match recent experimental evidence on the effect of local body curvature on nearby
38 motoneurons [6]. The neuromuscular system is embedded in a model of the physics of the worm's
39 body [10]. We used an evolutionary algorithm to explore the space of unknown parameters of the
40 head and VNC motoneuron circuits such that the integrated neuromechanical model matched
41 the speed of the worm during forward locomotion on agar. Analysis of successful solutions
42 suggests that sensory feedback mechanisms in the head motoneurons and the VNC are sufficient
43 to generate and propagate dorsoventral waves to produce forward locomotion behavior. Detailed
44 analysis of the operation of the model sheds further light on the mechanisms that generate and
45 propagate oscillations and leads to a number of experimental predictions.

46 Model

47 Environment properties

48 In the laboratory, *C. elegans* is typically grown and studied in petri dishes containing a layer of
49 agar gel. The gel is firm and worms tend to lie on the surface. The locomotion behavior observed
50 under these conditions is referred to as crawling. Worms are sometimes also studied in a liquid
51 medium such as water, leading to a related locomotion behavior called swimming [11]. The
52 experiments in this paper will focus only on agar gel. Given the low Reynolds number physics of
53 *C. elegans* locomotion, inertial forces can be neglected and the resistive forces of the medium can
54 be well-approximated as a linear drag $F = -Cv$ [10, 12, 13, 14]. Estimated values of the ratio for
55 drag coefficient for nematodes crawling on agar gels vary by as much as an order of magnitude
56 (ranging from 1.5 to 40) in the literature [11, 14, 15, 16, 17]. The tangential and normal drag
57 coefficients for agar used in this model were taken from those reported in [11] and used in the
58 model of the body that this work builds on [10]: $C_{\parallel} = 3.2 \times 10^{-3} \text{ kg}\cdot\text{s}^{-1}$ and $C_{\perp} = 128 \times 10^{-3}$
59 $\text{kg}\cdot\text{s}^{-1}$, respectively [10, 11, 12, 14, 18, 19].

60 Body model

61 The model of the body is a reimplementaion of the model presented by Boyle, Berri, and
62 Cohen [10]. The worm is modeled in 2D cross-section. This is justified because when placed on an
63 agar surface, the worm locomotes on its side, bending only in the dorsal-ventral plane. The $\sim 1\text{mm}$
64 long continuous body of the worm is divided into variable-width discrete segments (Fig. 1A),
65 each of which are bounded by two cross-sectional rigid rods whose endpoints are connected to
66 their neighbors via damped spring lateral elements modeling the stretch resistance of the cuticle
67 and damped spring diagonal elements modeling the compression resistance of internal pressure.
68 The rest lengths, spring constants and damping constants of the lateral and diagonal elements
69 are taken directly from previous work [10], who in turn estimated them from experiments with
70 anesthetized worms [20]. The forces from the lateral and diagonal elements are summed at the
71 endpoints of the rods and then the equations of motion are written for the center of mass of each
72 rod. The full set of expressions for forces are identical to those in [10, 12]. Since each rod has
73 two translational (x, y) and one rotational (ϕ) degrees of freedom, the body model has a total
74 of $3(N_{\text{seg}} + 1)$ degrees of freedom. The current model has $N_{\text{seg}} = 50$, so a total of 153 degrees of
75 freedom. All kinematic and dynamic parameters are identical to those used in [10, 12].

76 Muscles

77 Body wall muscles in the worm are arranged as staggered pairs in four bundles around the body
78 and are divided into 16 in the head, 16 in the neck and 63 in the rest of the body [2, 21]. These
79 muscles can contract and relax in the dorsoventral plane. Unlike previous work [10], we do not
80 directly associate each discrete lateral element of the body model with a distinct muscle. Instead,
81 muscles are modeled as separate damped springs that lie along the cuticle and their force is
82 distributed across all lateral elements that they intersect (Fig. 1B). This allows us to vary the spatial
83 resolution of the body discretization independently from the number of muscles. It also allows us
84 to accommodate the fact that adjacent body wall muscles overlap one another in *C. elegans*. Since
85 the model is 2D, we combine right and left bundles into a single set of 24 dorsal and 24 ventral
86 muscles, each with twice the strength. Following previous work [10], muscles are modeled as
87 damped springs with activation-dependent rest lengths, spring constants and damping constants,
88 endowing them with simplified Hill-like force-length and force-velocity properties [22]. Muscle
89 activation is modeled as a leaky integrator with a characteristic time scale ($\tau_M = 100\text{ms}$), which
90 crudely agrees with response times of obliquely striated muscle [23]. The muscle activation is
91 represented by the unitless variable $A_{M,m}^k$ that evolves according to

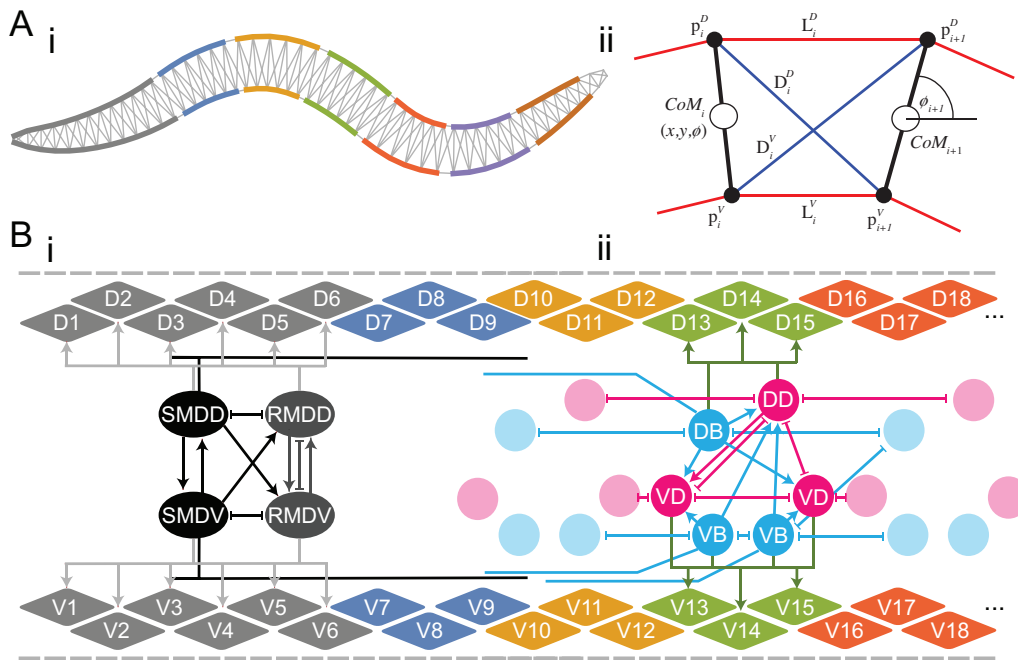


Figure 1. Neuromechanical model. [A] Physical model of the body adapted from [10]: (i) Complete model. Lateral elements are colored according to the muscles they are driven by. Head and neck muscles are driven by the head motoneuron circuit (gray) (see panel B(i)). The rest of the body wall muscles are driven by a series of 6 repeating VNC units (blue, orange, green, red, purple, and brown) (see panel B(ii)). (ii) One of 49 individual segments. Cross-sectional rigid rods (black), damped spring lateral elements (red), damped spring diagonal elements (blue). [B] Neuromuscular model. Dorsal and ventral lateral elements from the physical body represented in gray on the top and bottom, respectively. Dorsal and ventral staggered muscle arrangement. Muscle force is distributed across all lateral elements they intersect. (i) Head neuromuscular unit includes SMD (black) and RMD (gray) motoneurons that connect to muscles on each side. SMD-class neurons receive stretch-receptor input from self and posterior region covered by black process. (ii) One of 6 repeating VNC neuromuscular units, derived from a statistical analysis of the connectome [3]. Each unit includes one dorsal and two ventral B- (blue) and D-class (magenta) motoneurons that connect to muscles on each side. B-class neurons receive stretch-receptor input from anterior region covered by blue process [6]. Circuits include all chemical synapses (arrows), gap junctions (connections with line endings), and neuromuscular junctions.

$$\frac{dA_{M,m}^k}{dt} = \frac{1}{\tau_M} (I_{NMJ,m}^k - A_{M,m}^k) \quad (0.1)$$

92 where $I_{NMJ,m}^k$ is the total current driving the muscle. Also following previous modeling work [10]
 93 and experimental evidence that electrical coupling between body wall muscle cells only plays a
 94 restricted role for *C. elegans* body bend propagation [6, 24], inter-muscle electrical coupling is
 95 assumed to be too weak and therefore not included in the model.

96 Head motoneuron circuit

97 In the worm, the head and neck muscles are driven by a set of motoneuron classes that include:
 98 bilaterally symmetric RIM, RIV, RMF, RMG, RMH; fourfold symmetric RME, SMB, URA; and
 99 sixfold symmetric IL1 [1]. Of these, only four of them (RMD, RME, SMB, SMD) innervate both
 100 head muscles and neck muscles; the rest innervate either only the head region (IL1, RMF, RMH,
 101 URA) or only the neck region (RIM, RIV, RMG). Given the parallels between SMB and SMD,
 102 and between RMD and RME, our model considers only the SMD and RMD motoneurons for the

103 head motoneuron circuit. We used the connectome data to identify the chemical and electrical
104 synapses connecting the two motoneurons and how they innervate head and neck muscles
105 (Fig. 1B(i)). SMD and RMD motoneurons drive head and neck muscles, $m = [1, 6]$, according
106 to: $I_{\text{NMJ},m}^k = w_{\text{NMJ},\text{SMD}} S_{\text{SMD}} + w_{\text{NMJ},\text{RMD}} S_{\text{RMD}}$. We constrained the sign of their neuromuscular
107 junctions using data from the expression of neurotransmitters: SMD and RMD neuromuscular
108 junctions are both excitatory [25].

109 Repeating ventral nerve cord circuit

110 The rest of the muscles in the body are driven by eight classes of motor neurons: AS, DA,
111 DB and DD innervate the dorsal body wall muscles and VA, VB, VC and VD innervate the
112 ventral muscles. Of the VNC motoneurons, only the B- (DB and VB) and D- (DD and VD)
113 classes have been shown to be involved in forward locomotion, so our model includes them
114 only [6, 26, 27, 28, 29]. As connectome data is incomplete for the posterior half of the worm [1, 30],
115 we relied on a statistical analysis of the motoneurons in relation to the position of the muscles
116 they innervate to model a repeating neural unit along the VNC [3]. When specialized to the
117 B-class and D-class motoneurons, this leads to the circuit architecture shown in Figure 1B(ii).
118 We model 6 such repeating neural units along the VNC, with identical parameters. D- and B-
119 class motoneuron drive body wall muscles posterior to the head and neck, $m = [7, 24]$, according
120 to: $I_{\text{NMJ},m}^k = w_{\text{NMJ},\text{B}} S_{\text{B}} + w_{\text{NMJ},\text{D}} S_{\text{D}}$. Finally, because the B-class motoneurons are known to be
121 cholinergic and therefore excitatory and the D-class motoneurons are GABAergic and therefore
122 inhibitory [25, 31], we constrain the signs of their neuromuscular junctions accordingly.

123 Neural model

124 Following electrophysiological studies in *C. elegans* [32, 33] and previous modeling efforts [34, 35],
125 all motoneurons were modeled as isopotential nodes with the ability to produce regenerative
126 responses, according to:

$$\tau_i \frac{dy_i}{dt} = -y_i + \sum_{j=1}^N w_{ji} \sigma(y_j + \theta_j) + \sum_{j=1}^N g_{ji} (y_j - y_i) + r_i I_{\text{SR},i} \quad (0.2)$$

127 where y_i represent the membrane potential of the i^{th} neuron relative to its resting potential,
128 τ_i is the time constant, w_{ji} corresponds to the synaptic weight from neuron j to neuron i , g_{ji}
129 corresponds to the conductance between cell i and j ($g_{ji} > 0$), and r_i corresponds to the stretch
130 receptor influence to neuron i . The model assumes chemical synapses release neurotransmitter
131 tonically and that steady-state postsynaptic voltage is a sigmoidal function of presynaptic
132 voltage [36, 37, 38], $\sigma(x) = 1/(1 + e^{-x})$, where $\sigma(x)$ is the synaptic potential or output of the
133 neuron (S_i). The chemical synapse has two parameters: θ_j is a bias term that shifts the range
134 of sensitivity of the output function, and w_{ji} represents the strength of the chemical synapse.
135 Electrical or gap junctions between *C. elegans* neurons are common. In line with previous
136 models [35, 38, 39], the model assumes electrical synapses can be modeled as bidirectional
137 ohmic resistances. As we have shown previously [40], this neural model has the capacity to
138 reproduce qualitatively a wide range of electrophysiological properties observed in *C. elegans*
139 neurons [32, 33]. The model can reproduce the passive activity that has been observed in some
140 neurons, like for example, AVA. Through the increase of the strength of the self-connection (>4 ,
141 see [41]), the model is also capable of reproducing the bistable potentials found in some neurons,
142 like, for example RMD [33].

143 Stretch receptors

144 Mechanosensitive stretch receptor channels have long been postulated to exist in motoneurons.
145 There is evidence that supports their existence in interneurons [42, 43], as well as more recently
146 in VNC motoneurons as well [6].

147 In the head motoneuron circuit, the SMD class has long undifferentiated processes that
148 are distal to the regions where neuromuscular junctions are situated, before they eventually
149 terminate, which have been postulated to be stretch sensitive [1]. We model SMD-class
150 motoneuron stretch receptors as a relatively long-range connection spanning the neck muscles
151 and the muscles associated with the first VNC neural unit ($m = [4, 9]$) (Fig. 1B(i)), with the effect
152 that the head and neck regions bend in the same direction and shortly after the bending of the
153 neck and anterior-most body region. The stretch-receptor current for the SMD-class motoneuron
154 sums over contributions from a total of 14 mechanical elements associated with those muscles,

$$I_{\text{SR,SMD}}^k = \sum_{s=7}^{21} h_s^k \quad (0.3)$$

155 In the repeating neural units of the VNC, the B-class is one motoneuron that has been
156 postulated to mediate stretch-receptor feedback from the body. The long undifferentiated
157 processes running posteriorly have led previous models to assume stretch receptors covered a
158 wide range of muscle cells and that proprioceptive information traveled anteriorly. However,
159 more recent experimental work demonstrated that the effect has a much shorter range
160 than previously assumed and is in fact directed posteriorly, since the activity of each VB
161 and DB motoneuron is activated by ventral and dorsal bending of a more anterior region,
162 respectively [6]. In light of this evidence, we model B-class motoneuron stretch receptors as
163 short-range connections from the lengths of anterior muscles to the immediately posterior B-
164 class motoneurons, with the effect that posterior body regions are encouraged to bend in the
165 same direction and shortly after the bending of a neighboring anterior region (Fig. 1B(ii)). The
166 stretch-receptor current for the B-class motoneuron in unit n on the k th side, $I_{\text{SR,B}_n}^k$, sums
167 over contributions from the $S = 6$ mechanical elements anterior to the anterior-most muscle that
168 neuron innervates ($S_{0,n}$):

$$I_{\text{SR,B}_n}^k = \frac{1}{S} \sum_{s=S_{0,n}-1-S}^{S_{0,n}-1} h_s^k \quad (0.4)$$

169 The proposed mechanosensitive channels in these processes respond to the changes in length
170 associated with body bending. In line with previous work [10], stretch receptors are modeled as
171 a weighted linear function of muscle length,

$$h_s^k = \frac{L_{L,s}^k - L_{0L,s}}{L_{0L,s}} \quad (0.5)$$

172 where $L_{0L,s}$ is the segment rest length and $L_{L,s}^k$ is the current length of the k th side
173 (dorsal/ventral) of the s th segment. In line with recent findings [6], we allow the stretch receptor
174 conductance to generate a depolarizing response to compression and a polarizing response to
175 stretch, relative to the local segment resting length.

176 Numerical methods

177 The model was implemented in C++ and was solved by Euler integration with a
178 1ms step. The code for the model and the evolutionary algorithm can be found at
179 <https://github.com/edizquie/RoyalSociety2018>.

180 Evolutionary algorithm

181 Unknown model parameters were adjusted using a real-valued evolutionary algorithm. A search
182 begins with a random population of genetic strings that encode the unknown parameters of
183 the neural circuit model. Each individual is then assigned a fitness based on the quality of its
184 locomotion performance. Individuals are then selected to serve as parents for the next generation
185 with a probability related to their fitness. From the selected parents, a new generation of children
186 are then produced by randomly swapping portions of two parents (crossover) and making a small
187 modification to the values of the resulting array with values drawn from a Gaussian distribution
188 (mutation). Once a new population has been constructed in this manner, the entire process
189 of evaluation, selection and reproduction repeats until the population converges on highly fit
190 individuals.

191 A naive parameterization of our model would contain over 400 muscle, neural and stretch
192 receptor parameters. However, it makes little sense to work directly with such a large set
193 of unconstrained parameters. Instead, we imposed a variety of symmetries on the model in
194 order to reduce the number of parameters. We assumed: (a) dorsal/ventral symmetry in the
195 parameters where possible; (b) that the parameters in each VNC neural unit were identical;
196 and (c) that neurons from the same class had identical parameters. Altogether, the model
197 has 30 free parameters. 4 Biases, 4 time-constants, 4 self-connections, and 4 neuromuscular
198 junctions, one for each motoneuron class (class). 2 stretch-receptor gains for SMD and B
199 stretch-receptors. In the head motoneuron circuit, weights for: 3 chemical synapses (synapses
200 between SMD motoneurons, synapses from SMD to RMD motoneurons, synapses between
201 RMD motoneurons); 2 gap junctions (synapse between RMD motoneurons, synapses between
202 SMD and RMD). In the repeating VNC neural unit, weights for: 3 chemical synapses (synapses
203 from B- to D- motoneurons in the same side, synapses from B- to D- motoneurons on
204 opposite sides, and synapse between D- motoneurons); 1 gap junction within the unit (synapse
205 between D- class motoneurons); 3 gap junctions across units (synapses across neighboring
206 D-class motoneurons, synapses across neighboring B-class neurons, synapse on neighboring B-
207 class neurons on opposite sides). Some parameters were constrained to match experimental
208 observations. Specifically, the self-connection for RMD was constrained to > 4 to force the
209 model neuron to be bistable as observed experimentally [33] and neuromuscular junctions
210 were constrained to be positive or negative depending on data from the expression of their
211 neurotransmitters.

212 In order to evaluate the fitness of a solution, we measured the locomotion efficiency of the
213 entire neuromechanical model. Specifically, we optimized model worms to match the worm's
214 average velocity on agar, by maximizing

$$f = 1 - \left| \frac{\bar{v} - v}{\bar{v}} \right| \quad (0.6)$$

215 where v is the average velocity of the model worm measured over 50 simulated seconds
216 and \bar{v} is the average velocity of the worm ($\bar{v} = 0.22\text{mm/sec}$, based on the ranges reported
217 experimentally [44, 45, 46, 47]). We measure the average velocity of the model worm by
218 calculating the Euclidean distance from the location of the center of the model worm's body at
219 the beginning of a trial to the location of its center at the end of the trial.

220 Results

221 Evolving locomotion

222 Model reliably evolves to match the worm's speed

223 In order to identify circuits that produced forward locomotion, we ran the evolutionary algorithm
224 100 times using different random seeds. The fitness of the model worm was evaluated to
225 match the worm's average velocity on agar ($v = 0.22\text{mm/sec}$), based on the ranges reported

226 experimentally [44, 45, 46, 47]. From each evolutionary run, we selected the best individual. As
227 our main interest was to identify networks capable of closely matching the worm's behavior,
228 we focused only on the highest performing subset of solutions, namely those networks having
229 a fitness score of at least 0.95 ($n = 46$). All solutions in this subset generated forward thrust by
230 means of a dorsoventral undulation of the body. All further analysis was limited to this ensemble
231 of solutions.

232 Solutions in the ensemble reproduce characteristic features of worm's movement

233 The behavior of the models match not only the speed of the worm, but also the overall qualitative
234 kinematics of forward movement. When placed on agar, the models in the ensemble initiate
235 dorsoventral oscillations in the head and propagate them posteriorly, generating thrust against
236 their environment, propelling themselves forward (see movie in Supplementary material). The
237 models can do this robustly, regardless of the initial state and posture of the worm, including
238 from a straight posture. The movement of the model worms resembles the worm's characteristic
239 frequency and its wavelength on agar. The ensemble of high-performance solutions locomote
240 with frequencies in the range [0.34, 0.43] and wavelengths in [0.70, 0.96], which are within the
241 range of what has been described in the literature: [0.25, 0.58] [11, 44, 46, 47, 48, 49] and [0.45,
242 0.83] [11, 44, 46, 47, 48, 49, 50, 51, 52, 53], respectively. That the solutions in the ensemble reproduce
243 characteristic features of the worm's movement that they were not evolved to match suggests
244 the model captures fundamental principles of the neuromechanical basis for the behavior in the
245 worm.

246 Individual Solution

247 In order to understand how oscillations are generated and propagated in the model worms, we
248 first consider the operation of one representative individual solution in detail (model parameters
249 in Supplementary material).

250 Head motoneuron circuit can generate oscillations using stretch-receptor feedback

251 Unlike previous models, the current model makes no explicit a priori assumption about where
252 oscillations should originate. As with the worm, curvature along the body of the model worm
253 over time during forward locomotion suggests the oscillation originates in the head and is
254 propagated posteriorly (Fig. 2A). In order to test whether the head motoneuron circuit can
255 generate oscillations, we silenced motoneurons in the VNC. Even in the absence of oscillatory
256 activity in the VNC, the head could still oscillate (Fig. 2B).

257 During regular forward locomotion, motoneurons in the head circuit of the model worm
258 oscillate (Fig. 2C). How are these oscillations generated? To address this question, we first silenced
259 stretch-receptors feedback in the head. When we silence stretch-receptor feedback to the head
260 motoneuron circuit, the neural oscillations in the head motoneuron circuit cease. Therefore,
261 despite the capacity of the head motoneuron circuit to generate intrinsic network oscillations, the
262 model worm produces oscillations robustly through stretch-receptor feedback. Such a reflexive
263 pattern generator hypothesis for oscillations in the head motoneuron circuit had only been
264 considered in two other models previously [49, 54]. We examine the differences between previous
265 models and the current model in detail in the Discussion.

266 In order to understand how the oscillation is generated through stretch-receptor feedback, we
267 consider the neural traces of the head motoneurons, stretch-receptor feedback, muscle activation,
268 and posture of the body over time during a full cycle of locomotion (Fig. 2C-E). At the start of a
269 cycle (stage i), the head and neck sections are straight (Fig. 2Di), SMD's undifferentiated process
270 is stretched and compressing, SMDD is off and RMDD is on (Fig. 2Ei). RMDD activates the dorsal
271 head and neck muscles and inhibits the contralateral RMDV motoneuron. As a result, the dorsal
272 head and neck segments contract, while the ventral segments expand, leading to a dorsal head
273 sweep, and the start of stage ii (Fig. 2Eii). Dorsal contraction in the anterior region of the body

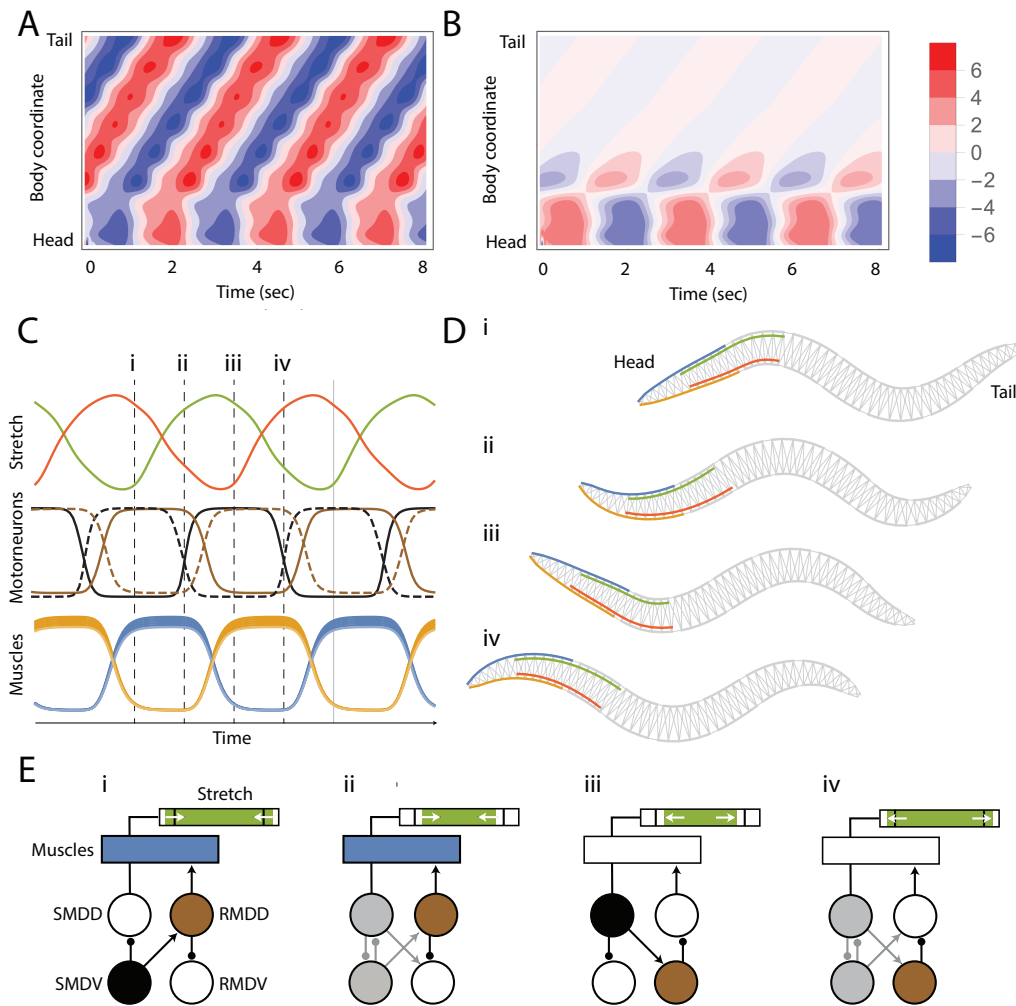


Figure 2. Oscillations in the head motoneuron circuit. [A] Kymogram during normal operation: Oscillation originates in the head and travels posteriorly. [B] Kymogram with VNC motoneurons silenced: Dorsoventral bends persist in head and neck. [C] Traces from stretch receptors, motoneurons, and muscles. Green/red traces dorsal/ventral stretch receptors. Black/brown traces SMD/RMD neural activity. Solid/dashed lines represent dorsal/ventral motoneurons. Blue/orange represents muscle activity from the 6 head and neck dorsal/ventral muscles. Activity is cyclic so four points are chosen in the cycle: i-iv. [D] Postures at the four instances of time selected in panel C. Dorsal/ventral head and neck muscles represented in blue/orange. Dorsal/ventral undifferentiated processes providing stretch information represented in green/red. [E] Mechanics of oscillation. Green bar represents amount of stretch/contraction in the dorsal undifferentiated process with respect to resting state (black vertical line). White arrows represent whether the process is stretching or compressing. Blue rectangle represents the dorsal head and neck muscles. Only dorsal muscles and stretch receptors are shown. The circles below represent the motoneurons. Muscles/neurons are filled in with color when they are contracted/activated and no color when they are relaxed/inactivated. The shade of gray represents the SMD neuron mid-activation. SMD motoneurons are shown in black and RMD motoneurons are shown in brown. Synapses appear only when they are in use.

274 leads to activation of the SMDD motoneuron through stretch-receptor feedback, which inhibits
 275 SMDV and excites RMDV, causing RMDV to deactivate. Deactivation of RMDV allows the dorsal
 276 muscle to begin to relax, and leads to stage iii (Fig. 2Eiii). Stage iii is dorsoventrally symmetric
 277 to stage i: the posture of the head and neck are straight, but the state of the neurons are flipped

278 in the dorsoventral dimension. SMDD is now on, and as a result SMDV is off and RMDV is on,
279 which results in RMDD being off. This means the ventral muscles are contracting and the dorsal
280 muscles are relaxing, leading to a ventral head sweep, and the start of stage iv (Fig. 2Eiii). Stage
281 iv is dorsoventrally symmetric to stage ii: the relaxing dorsal segments leads to inactivation of
282 SMDD, which ceases to inhibit SMDV and ceases to excite RMDV. Again together re-activation of
283 SMDV and re-inactivation of RMDV lead to the re-activation of RMDD, which leads to the dorsal
284 muscles contracting again, and the head and neck posture to get back to straight.

285 Oscillatory wave can be propagated posteriorly through stretch receptor feedback and 286 without bistable motoneurons

287 How is the oscillation that is generated in the head then propagated posteriorly to produce
288 the sinusoidal traveling wave responsible for forward thrust in the model worm? In order
289 to understand the operation of the repeating VNC circuit, we start by simplifying the circuit
290 architecture. Although neural traces suggest B- and D- class motoneurons are active, silencing
291 D-class motoneurons does not affect locomotion performance. Silencing B-class motoneurons
292 or removing the stretch-receptor feedback causes the propagation of the wave to cease. This
293 suggests we can simplify this circuit to only the B-class motoneurons for analysis of the wave
294 propagation. With this simplification, the operation of the VNC circuit is straightforward. As
295 the length of the segment anterior to the neural unit compresses, the stretch receptor excites the
296 motoneuron, activating the muscle, and ultimately causing the contraction of its own segment.
297 We can see this on the ventral side in stages ii and iii, and on the dorsal side on stages iv and i
298 (Fig. 3, panels B and C). Therefore, B-class motoneurons with input from stretch-receptors with
299 information about the length of the anterior regions of the body are the primary drivers of the
300 propagation of the rhythmic wave in this solution. Interestingly, B-class motoneurons are not
301 bistable. Therefore, provided the directionality of stretch-receptor feedback shown in [6], bistable
302 motoneurons are not essential for sustaining proprioceptively driven dorsoventral undulations
303 in the model. However, there are two other components that play roles in the propagation
304 of the wave: the inter-unit gap junctions, and the mechanics of the body. We characterize the
305 contribution of each component individually next.

306 Inter-unit gap junctions dampens curvature

307 In the model worm, the propagation of the oscillatory wave from the head to the first unit of
308 the VNC occurs through stretch receptors exclusively, as there are no direct synapses between
309 the head motoneuron circuit and the VNC motoneurons. However, the rest of the VNC units
310 are interconnected by electrical gap junctions between neighboring B-cells (see Fig. 1B). What
311 role do the gap junctions play in transferring the wave posteriorly from the first VNC to
312 the rest of them? When we silenced gap junctions between neighboring units, the wave still
313 travelled posteriorly. Interestingly, the amplitude of the dorsoventral curvature increased by 22%.
314 This suggests gap junctions are responsible for dampening the strength of the curvature. This
315 dampening is functional for forward locomotion: without inter-unit gap junctions, the speed
316 of the model worm dropped to 88.7% of its original speed. In terms of the worm's movement,
317 although the frequency of the oscillations remained relatively unaffected, the wavelength became
318 smaller: from 0.81 to 0.68. Altogether, this suggests that when the wave travels through stretch-
319 receptor feedback alone, it travels fast, and the gap junctions between neighboring units act to
320 dampen the wave through tighter communication with the motoneurons. Altogether, while the
321 inter-unit gap junctions play a role in the propagation of the wave, they are not essential for
322 producing forward movement.

323 Wave also propagates through the mechanical body

324 One of the benefits of a neuromechanical model is that we can study the effect of the mechanical
325 properties of the body on the operation of the behavior. So what role does the body mechanics

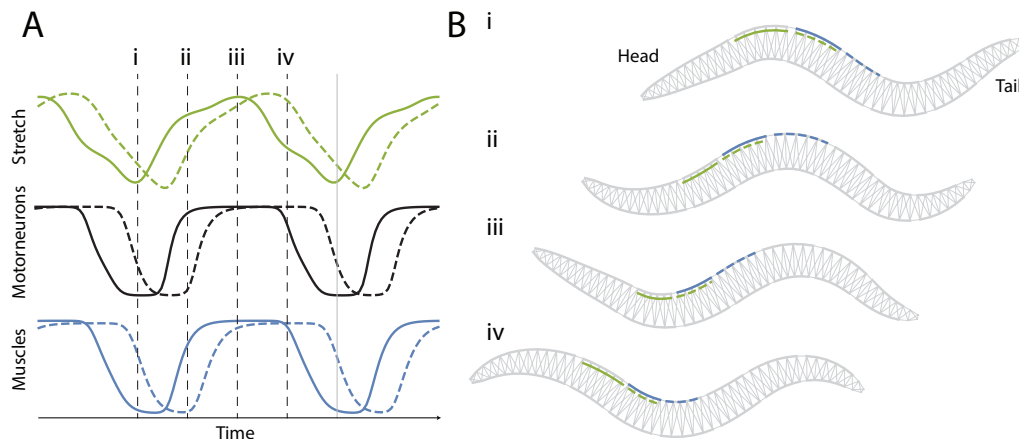


Figure 3. Wave propagation through stretch reception. [A] Traces from the dorsal stretch receptors (green), DB motoneurons (black), and dorsal muscles (blue) in two neighboring VNC neural units: second (solid) and third (dashed). The activity is cyclic so the same four unique points used for Figure 2 were chosen to analyze the wave propagation: i-iv (vertical dashed lines). [B] Worm postures at the four instances of time selected in panel A. The second VNC neural unit receives dorsal stretch receptor input from the solid green region and innervates the muscles in the solid blue region. The third VNC neural unit (posterior to the second), receives dorsal stretch receptor input from the dashed green region and innervates the muscles in the dashed blue region.

326 play in the wave propagation in the model worm? In order to address this question, we silenced
 327 the motoneuron activity of each neural unit individually, including the incoming stretch receptor
 328 feedback, and the gap junction connections with the unit anterior and posterior to them. Despite
 329 the silencing of entire neural units in the VNC, the model worm could still move forward
 330 (Fig. 4A). That is, the model worm can recover the traveling wave in the absence of the ventral
 331 nerve units from the passive propagation of the wave through the mechanical body. This is
 332 because mechanical curvature in one area of the worm forces curvature of neighboring segments.
 333 The combination of stretch-receptor feedback and passive mechanical propagation is sufficiently
 334 strong that even entirely disabling two adjacent VNC neural units does not impair the ability of a
 335 posterior VNC unit from picking up the remains of the traveling wave and re-establishing regular
 336 dorsoventral undulations (Fig. 4B).

337 Ensemble of solutions

338 In the individual solution analyzed in detail, the model moved forward in the absence of an
 339 intrinsic network oscillator in either the head motoneuron circuit or the VNC. Instead, oscillations
 340 were generated and propagated using stretch-receptor feedback with mechanical propagation
 341 playing a substantial role and electrical coupling playing a secondary role. In this section, we
 342 analyze how representative that solution is with respect to the rest of the solutions in the
 343 ensemble.

344 Wave originates in the head via stretch-receptor feedback or intrinsic network 345 oscillators

346 All solutions in the ensemble come to a stop when head motoneurons are silenced (orange,
 347 Fig. 5A). Yet, when VNC motoneurons are silenced, the head continues to oscillate (green, Fig. 5B),
 348 moving forward at a fraction of the speed (green, Fig. 5A). Therefore, in all solutions, the head
 349 motoneuron circuit generates oscillations that are used for moving forward. In 40 of the 46
 350 solutions in the ensemble, oscillations in the head ceased when we silenced stretch-receptor

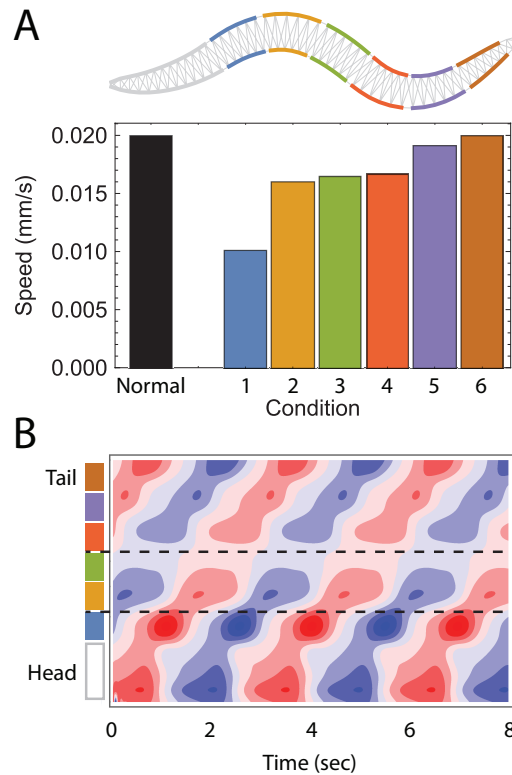


Figure 4. Role of biomechanics in the propagation of the wave and locomotion. [A] Speed of the worm as a result of silencing entire VNC neural units. Color coding according to the region of the body those neural units affect. Black represents the speed of the model worm under normal conditions. Propagation of the wave does not depend entirely on stretch-receptor feedback and neural activity in general. [B] Example kymogram of movement while two VNC neural units (2 and 3) have been silenced. Despite the lack of neural activity, and the lack of network oscillators in the tail, there are oscillations in the head and tail.

351 feedback to the head motoneuron circuit (red, Fig. 5B). The remaining 6 solutions generate
352 intrinsic network oscillations in the absence of stretch-receptor feedback. These oscillations were
353 sufficient to drive regular forward locomotion (red, Fig. 5A). This suggests the architecture of
354 the head motoneuron circuit can generate oscillations to drive forward locomotion equally well
355 either through intrinsic network oscillations or through stretch-receptor feedback. In both types
356 of solutions, both SMD and RMD motoneurons were essential for producing forward movement
357 throughout the ensemble.

358 Oscillatory wave is propagated posteriorly through stretch receptor feedback

359 The way the wave is propagated posteriorly in the ensemble of solutions resembles closely that
360 of the model worm analyzed individually. In order to analyze wave propagation in the ensemble
361 of solutions, we silenced the main components of the VNC while measuring the speed of the
362 worm as well as the average magnitude of the dorsoventral bends along the VNC region of the
363 body (Fig. 6). We summarize the main results ahead. First, the B-class motoneuron is essential
364 for forward locomotion in all solutions. Silencing B-class motoneurons eliminates dorsoventral
365 rhythmic patterns along the body and results in model worms coming to a full stop. Second,
366 B-class motoneurons did not evolve to be bistable in any of the solutions. Therefore, bistable
367 motoneurons are not essential for sustaining proprioceptively driven dorsoventral undulations
368 in the model. Third, silencing stretch-receptor feedback input into the B-class motoneurons also

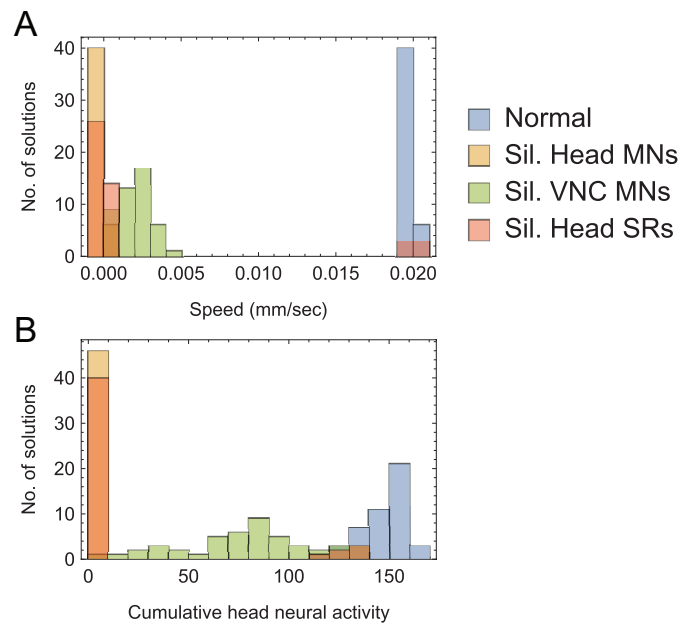


Figure 5. Operation of the head motoneuron circuit in the ensemble of solutions. Distribution of speed [A] and magnitude of change in neural activity in head motoneurons [B] of all model worms in the ensemble under different conditions: Normal locomotion (blue), when head motoneurons are silenced (orange), when VNC motoneurons are silenced (green), when head stretch-receptor feedback is silenced (red).

369 eliminates dorsoventral rhythmic patterns along the body and results in model worms coming to
370 a full stop. Therefore, as with the model worm analyzed individually, stretch receptor feedback is
371 essential for propagating the wave posteriorly. Fourth, in 41 of the 46 solutions in the ensemble,
372 the D-class motoneuron was not essential for forward locomotion. In these solutions, silencing the
373 D-class motoneurons does not affect speed or dorsoventral bends. In the remaining 5 solutions,
374 the D-class is involved in contralateral inhibition and is essential for wave propagation. Fifth, the
375 inter-unit neighboring gap junctions play a minor role in the propagation of the wave. Removing
376 neighboring gap junction augments the strength of the curvature, yet this increase in curvature
377 leads to impaired movement. Finally, the biomechanics of the body alone plays a substantial
378 role in propagating the wave posteriorly. Silencing entire neural units in the VNC does not
379 entirely disrupt propagation of the wave posteriorly. Although silencing entire neural units affects
380 the speed, the model worms still move forward. As with the solution analyzed individually,
381 impairing anterior units has a larger effect than impairing posterior units.

382 Discussion

383 We have presented a fully integrated, biologically and physically grounded model that accounts
384 for *C. elegans* locomotion on agar that takes into consideration the head motoneuron circuit and
385 the ventral nerve cord motoneuron circuit. The model was motivated by findings regarding the
386 range and directionality of local body curvature on motoneurons [6] and the statistical analysis
387 of the repeating structure of the VNC [3]. With these biological constraints provided, we used
388 an evolutionary algorithm to systematically explore the space of possibilities for generating
389 locomotion. We discuss ahead key insights revealed from the analysis of evolved solutions and
390 related work.

391 We have demonstrated that a model of the head motoneuron circuit with SMD and
392 RMD alone is sufficient to generate oscillations that can drive dorsoventral undulations in the

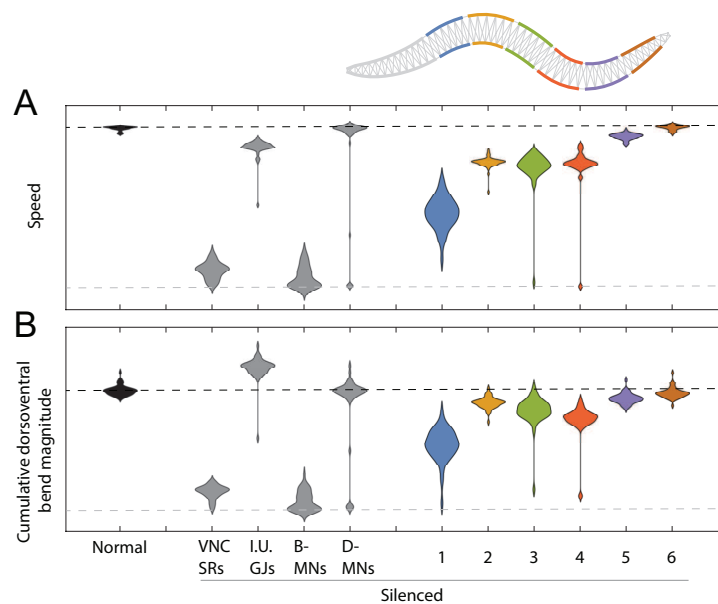


Figure 6. Operation of the VNC in the ensemble of solutions. Distribution of speed [A] and magnitude of dorsoventral bends [B] of all model worms in the ensemble under different conditions: Normal locomotion (black), when VNC stretch-receptor feedback, interunit gap junctions, B-class, and D-class motoneurons are silenced independently (gray), and when an entire neural unit is silenced (colored according to position along the body). The black dashed lines represents the value expected of a normally moving model worm; the gray dashed line represents the value expected of a non-moving model worm.

393 head and neck. Analysis of the variations in the ensemble of solutions revealed two possible
 394 mechanisms: an intrinsic network oscillator and an oscillator driven by stretch-receptor feedback
 395 with information about the length of the region posterior to the SMD motoneuron. Furthermore,
 396 the co-existence of both mechanisms in the worm would be feasible.

397 Our model integrates the head motoneuron circuit and the VNC motoneuron circuit within
 398 a physical model of the body and environment, such that the forward motion of the model
 399 emerges from the undulation of the body. Although a number of computational models had
 400 considered the head motoneuron circuit in the absence of a physical framework of the body and
 401 environmental forces [49, 54, 55, 56], previous neuro-mechanical models of forward locomotion
 402 had either assumed an oscillator in the head [14] or modeled the head circuit as an additional
 403 VNC unit [10]. The reflexive pattern generator hypothesis for oscillations in the head circuit that
 404 emerged from our evolutionary experiments had been considered in two previous models [49, 54].
 405 We highlight here the most substantive differences between these two previous models and the
 406 one proposed here. First, in previous models the circuit responsible for oscillations included
 407 a broad range of head interneurons and motoneurons. In the Sakata and Shingai model [54],
 408 these classes include AIB, AIZ, AVB, AVK, RIA, RIB, RIC, RIG, RIS, RIV, RMD, RME, SAA, SMB,
 409 and SMD. In the Karbowski et al. model [49], the neurons were identified more abstractly as
 410 one of several possible head interneurons subsets, including AIZ, AIA, AWA, and AIZ or RIB,
 411 RIG, URY, and RIB, SAA, and head motoneurons including one of either SMB or SMD, and
 412 RME. In contrast, in the current model we demonstrate that a minimal set of head motoneurons
 413 (specifically SMD and RME) are sufficient to generate oscillations. Second, in the previous models
 414 the stretch receptor feedback into the head interneurons was postulated to come from SAA
 415 and was thus modeled to receive stretch information from the head posture. In contrast, the
 416 current model postulates that stretch receptor feedback from SMD is sufficient to drive oscillations
 417 in the head using postural information from regions in the head and posterior to the head.

418 Third, in the previous models the oscillations in the head circuit were imposed downstream
419 premotor command interneurons (e.g., AVB and PVC), which were then communicated to VNC
420 motoneurons. However, the activity of these neurons has since been demonstrated not to
421 correlate with locomotion undulations [27, 29]. In contrast, in the current model we demonstrate
422 that the oscillations in the head motoneurons can be propagated to the VNC motoneurons
423 through stretch-receptor feedback. Finally, in previous models the parameters of the head
424 circuit were hand-designed to generate oscillations. In the current model, we do not assume
425 that oscillations can only be generated in the head; oscillations in the head emerge from the
426 evolutionary optimization process given the neuroanatomical constraints.

427 We have demonstrated that a neuro-mechanical model of the worm with short-range and
428 posteriorly directed proprioceptive feedback in the VNC is sufficient to propagate the wave
429 along the body and produce forward locomotion. A key component in our model is that we
430 allow the stretch receptor conductance to generate a depolarizing response to compression and
431 a polarizing response to stretch, relative to the local segment resting length, in line with recent
432 findings [6]. A detailed analysis of the solutions revealed five key mechanisms for sustaining the
433 proprioceptively driven dorsoventral undulations in the model. (a) The dorsoventral undulation
434 generated in the head motoneuron circuit is propagated posteriorly to the VNC, despite the
435 lack of direct synapses between the head motoneurons and VNC motoneurons, through stretch-
436 receptor feedback from the anterior-most VNC neural unit. (b) The wave is propagated along
437 the rest of the VNC neuromuscular units primarily through stretch-receptor feedback from the
438 region immediately anterior to it. (c) Bistable motoneurons are not necessary for sustaining the
439 proprioceptively driven dorsoventral undulations in the model. (d) Despite the role of stretch-
440 receptor feedback, the inclusion of a biomechanical model revealed that the passive mechanics of
441 the body play a substantial role in the propagation of the undulation, in the absence of entire
442 subregions of the VNC. (e) The contribution from the inter-unit gap junctions was relatively
443 minor, serving mostly to dampen curvature. The proposed model is consistent with the recent
444 findings that in the absence of AVB-B gap junction inputs driving B-class motoneurons to intrinsic
445 oscillatory activity, proprioceptive couplings can still propagate bending waves throughout the
446 majority of the length of the body [57]. All of these postulated mechanisms would be promising
447 to investigate further experimentally.

448 Despite the breadth of knowledge about the neurobiology, anatomy and physics of *C.*
449 *elegans*, there are still a number of unanswered questions about the neuromechanical basis
450 of one of its most basic behaviors. Our model proposes a head motoneuron circuit that can
451 generate oscillations and a VNC motoneuron circuit that can propagate the wave using stretch-
452 receptor feedback in a mechanical model of the body, altogether sufficient to propel the worm
453 forward in agar. Furthermore, we demonstrate a methodology to systematically explore different
454 mechanisms that match behavior given biological assumptions. Further work will involve
455 matching the behavior of the integrated neuromechanical model to the effect produced from
456 optogenetic and physical manipulations reported in recent experiments [57, 58]. Ultimately,
457 improving our understanding of forward locomotion will allow us to study more complex
458 behaviors that may require contributions from additional neural circuits.

459 Acknowledgments

460 The work in this paper was supported in part by NSF grant IIS-1524647.

461 References

- 462 1 JG White, E Southgate, JN Thomson, and S Brenner. The structure of the nervous system of
463 the nematode *Caenorhabditis elegans*. *Philos Trans R Soc Lond B Biol Sci*, 275(938):327–348, 1986.
- 464 2 RH Waterston. Muscle. In WB Wood, editor, *The nematode C. elegans*, pages 281–335. Cold
465 Spring Harbor Laboratory Press, New York, 1988.

- 466 3 G Haspel and MJ O'Donovan. A perimotor framework reveals functional segmentation in
467 the motoneuronal network controlling locomotion in *Caenorhabditis elegans*. *J Neurosci*, 31(41):
468 14611–14623, 2011.
- 469 4 P Babington. *C. elegans II*. Cold Spring Harbour Laboratory Press, New York, 2 edition, 1997.
- 470 5 N Tavernarakis, W Shreffler, S Wang, and M Driscoll. unc-8, a deg/enac family member,
471 encodes a subunit of a candidate mechanically gated channel that modulates *C. elegans*
472 locomotion. *Neuron*, 18:107–119, 1997.
- 473 6 Q Wen, MD Po, E Hulme, S Chen, X Liu, SW Kwok, M Gershow, AM Leifer, V Butler, C Fang-
474 Yen, et al. Proprioceptive coupling within motor neurons drives *C. elegans* forward locomotion.
475 *Neuron*, 76(4):750–761, 2012.
- 476 7 J Gjorgjieva, D Biron, and G Haspel. Neurobiology of *Caenorhabditis elegans* locomotion: where
477 do we stand? *Bioscience*, 64(6):476–486, 2014.
- 478 8 N Cohen and T Sanders. Nematode locomotion: dissecting the neuronal–environmental loop.
479 *Curr Opin Neurobiol*, 25:99–106, 2014.
- 480 9 M Zhen and ADT Samuel. *C. elegans* locomotion: small circuits, complex functions. *Curr Opin*
481 *Neurobiol*, 33:117–126, 2015.
- 482 10 JH Boyle, S Berri, and N Cohen. Gait modulation in *C. elegans*: an integrated neuromechanical
483 model. *Front Comput Neurosci*, 6:10, 2012. doi: 10.3389/fncom.2012.00010.
- 484 11 S Berri, JH Boyle, M Tassieri, IA Hope, and N Cohen. Forward locomotion of the nematode *C.*
485 *elegans* is achieved through modulation of a single gait. *HFSP J*, 3(3):186–193, 2009.
- 486 12 JH Boyle. *C. elegans locomotion: An integrated approach*. PhD thesis, University of Leeds, 2010.
- 487 13 N Cohen and JH Boyle. Swimming at low reynolds number: a beginner's guide to undulatory
488 locomotion. *Contemporary Physics*, 51:103–123, 2010.
- 489 14 E Niebur and P Erdős. Theory of the locomotion of nematodes: Dynamics of undulatory
490 progression on a surface. *Biophys J*, 60(5):1132–1146, 1991.
- 491 15 J Karbowski, CJ Cronin, A Seah, JE Mendel, D Cleary, and PW Sternberg. Conservation rules,
492 their breakdown, and optimality in *Caenorhabditis* sinusoidal locomotion. *Journal of Theoretical*
493 *Biology*, 242(3):652 – 669, 2006. ISSN 0022-5193. doi: 10.1016/j.jtbi.2006.04.012.
- 494 16 P Sauvage, M Argentina, J Drappier, T Senden, J. Simão, and JM Di Meglio. An elasto-
495 hydrodynamical model of friction for the locomotion of *Caenorhabditis elegans*. *Journal of*
496 *Biomechanics*, 44(6):1117 – 1122, 2011. ISSN 0021-9290. doi: 10.1016/j.jbiomech.2011.01.026.
- 497 17 R Rabets, M Backholm, K Dalnoki-Veress, and WS Ryu. Direct measurements of drag forces in
498 *C. elegans* crawling locomotion. *Biophysical Journal*, 107(8):1980 – 1987, 2014. ISSN 0006-3495.
499 doi: 10.1016/j.bpj.2014.09.006.
- 500 18 J Lighthil. Flagellar hydrodynamics. *SIAM Rev*, 18:161–230, 1976.
- 501 19 HR Wallace. Wave formation by infective larvae of the plant parasitic nematode *Meloidogyne*
502 *javanica*. *Nematologica*, 15(1):65–75, 1969.
- 503 20 P Sauvage. *Etude de la locomotion chez C. elegans et perturbations mecaniques du mouvement*. PhD
504 thesis, Universite Paris, 2007.
- 505 21 ZF Altun and DH Hall. Muscle system, somatic muscle. In *WormAtlas*. 2009.
506 doi:10.3908/wormatlas.1.7.
- 507 22 AV Hill. The heat of shortening and the dynamics constants of muscle. *Proc. R. Soc. London B*,
508 126:136–195, 1938.
- 509 23 B Milligan, N Curtin, and Q Bone. Contractile properties of obliquely striated muscle from
510 the mantle of squid (*Alloteuthis subulata*) and cuttlefish (*Sepia officinalis*). *J Exp Biol*, 200(Pt 18):
511 2425–24236, 1997.
- 512 24 AM Leifer, C Fang-Yen, M Gershow, MJ Alkema, and ADT Samuel. Optogenetic manipulation
513 of neural activity in freely moving *Caenorhabditis elegans*. *Nature Methods*, 8:147–152, 2011. doi:
514 10.1038/nmeth.1554.
- 515 25 JB Rand and ML Nonet. Neurotransmitter assignments for specific neurons. In *C. elegans II*,
516 pages 1049–1052. Cold Spring Harbour Laboratory Press, New York, 1997.
- 517 26 M Chalfie, JE Sulston, JG White, E Southgate, JN Thomson, and S Brenner. The neural circuit
518 for touch sensitivity in *Caenorhabditis elegans*. *J Neurosci*, 5(4):956–964, 1985.

- 519 27 S Faumont, G Rondeau, TR Thiele, KJ Lawton, KE McCormick, M Sottile, O Griesbeck,
520 ES Heckscher, WM Roberts, CQ Doe, et al. An image-free opto-mechanical system for creating
521 virtual environments and imaging neuronal activity in freely moving *Caenorhabditis elegans*.
522 *PLoS One*, 6(9):e24666, 2011. doi: 10.1371/journal.pone.0024666.
- 523 28 G Haspel, MJ O'Donovan, and AC Hart. Motoneurons dedicated to either forward or
524 backward locomotion in the nematode *Caenorhabditis elegans*. *J Neurosci*, 30(33):11151–11156,
525 2010.
- 526 29 T Kawano, MD Po, S Gao, G Leung, WS Ryu, and M Zhen. An imbalancing act: gap junctions
527 reduce the backward motor circuit activity to bias *C. elegans* for forward locomotion. *Neuron*,
528 72(4):572–586, 2011.
- 529 30 LR Varshney, BL Chen, E Paniagua, DH Hall, and DB Chklovskii. Structural properties of the
530 *Caenorhabditis elegans* neuronal network. *PLoS Comput Biol*, 7(2):e1001066, 2011. doi: 10.1371/
531 journal.pcbi.1001066.
- 532 31 SL McIntire, E Jorgensen, J Kaplan, and HR Horvitz. The gabaergic nervous system of
533 *Caenorhabditis elegans*. *Nature*, 364(6435):337–41, 1993.
- 534 32 SR Lockery and MB Goodman. The quest for action potentials in *C. elegans* neurons hits a
535 plateau. *Nat Neurosci*, 12(4):377–378, 2009.
- 536 33 JE Mellem, PJ Brockie, DM Madsen, and AV Maricq. Action potentials contribute to neuronal
537 signaling in *C. elegans*. *Nat Neurosci*, 11(8):865–867, 2008.
- 538 34 EJ Izquierdo and SR Lockery. Evolution and analysis of minimal neural circuits for klinotaxis
539 in *Caenorhabditis elegans*. *J Neurosci*, 30(39):12908–12917, 2010.
- 540 35 EJ Izquierdo and RD Beer. Connecting a connectome to behavior: an ensemble of
541 neuroanatomical models of *C. elegans* klinotaxis. *PLoS Comput Biol*, 9(2):e1002890, 2013. doi:
542 10.1371/journal.pcbi.1002890.
- 543 36 M Kuramochi and M Doi. A computational model based on multi-regional calcium imaging
544 represents the spatio-temporal dynamics in a *Caenorhabditis elegans* sensory neuron. *PLoS One*,
545 12(1):e0168415, 2017. doi: 10.1371/journal.pone.0168415.
- 546 37 TH Lindsay, TR Thiele, and SR Lockery. Optogenetic analysis of synaptic transmission in the
547 central nervous system of the nematode *Caenorhabditis elegans*. *Nat Commun*, 2(306), 2011. doi:
548 10.1038/ncomms1304.
- 549 38 SR Wicks, CJ Roehrig, and CH Rankin. A dynamic network simulation of the nematode
550 tap withdrawal circuit: predictions concerning synaptic function using behavioral criteria. *J*
551 *Neurosci*, 16(12):4017–4031, 1996.
- 552 39 JM Kunert, JL Proctor, SL Brunton, and JN Kutz. Spatiotemporal feedback and network
553 structure drive and encode *Caenorhabditis elegans* locomotion. *PLoS Comput Biol*, 13(1):
554 e1005303, 2017. doi: 10.1371/journal.pcbi.1005303.
- 555 40 EO Olivares, EJ Izquierdo, and RD Beer. Potential role of a ventral nerve cord central pattern
556 generator in forward and backward locomotion in *Caenorhabditis elegans*. *Network Neuroscience*,
557 0(ja):1–32, 2017. doi: 10.1162/NETN_a__00036.
- 558 41 RD Beer. On the dynamics of small continuous-time recurrent neural networks. *Adapt Behav*,
559 3(4):469–509, 1995.
- 560 42 W Li, Z Feng, PW Sternberg, and XZS Xu. A *C. elegans* stretch receptor neuron revealed by a
561 mechanosensitive trp channel homologue. *Nature*, 440:684–687, 2006.
- 562 43 WR Schafer. Proprioception: a channel for body sense in the worm. *Curr. Biol.*, 16:R509–R511,
563 2006.
- 564 44 XN Shen, J Sznitman, P Krajacic, T Lamitina, and PE Arratia. Undulatory locomotion of
565 *Caenorhabditis elegans* on wet surfaces. *Biophysical Journal*, 102(12):2772–2781, 2012. doi:
566 10.1016/j.bpj.2012.05.012.
- 567 45 DT Omura, DA Clark, ADT Samuel, and HR Horvitz. Dopamine signaling is essential for
568 precise rates of locomotion by *C. elegans*. *PLOS ONE*, 7(6):1–9, 06 2012. doi: 10.1371/journal.
569 pone.0038649.
- 570 46 E Cohen, E Yemini, W Schafer, DG Feitelson, and M Treinin. Locomotion analysis identifies
571 roles of mechanosensory neurons in governing locomotion dynamics of *C. elegans*. *Journal of*
572 *Experimental Biology*, 215(20):3639–3648, 2012. doi: 10.1242/jeb.075416.

- 573 47 CJ Cronin, JE Mendel, S Mukhtar, YM Kim, RC Stirbl, J Bruck, and PW Sternberg. An
574 automated system for measuring parameters of nematode sinusoidal movement. *BMC*
575 *Genetics*, 6(5), 2005. doi: 10.1186/1471-2156-6-5.
- 576 48 C Fang-Yen, M Wyart, J Xie, R Kawai, T Kodger, S Chen, and ADT Samuel. Biomechanical
577 analysis of gait adaptation in the nematode *Caenorhabditis elegans*. *Proceedings of the National*
578 *Academy of Sciences of the United States of America*, 107(47):20323–20328, 2010. doi: 10.1073/pnas.
579 1003016107.
- 580 49 J Karbowski, G Schindelman, CJ Cronin, A Seah, and PW Sternberg. Systems level circuit
581 model of *C. elegans* undulatory locomotion: mathematical modeling and molecular genetics. *J*
582 *Comput Neurosci*, 24(3):253–276, 2008.
- 583 50 JT Pierce-Shimomura, BL Chen, JJ Mun, R Ho, R Sarkis, and SL McIntire. Genetic analysis
584 of crawling and swimming locomotory patterns in *C. elegans*. *Proceedings of the National*
585 *Academy of Sciences of the United States of America*, 105(52):20982–20987, 2008. doi: 10.1073/
586 pnas.0810359105.
- 587 51 E Yemini, T Jucikas, LJ Grundy, AEX Brown, and WR Schafer. A database of *C. elegans*
588 behavioral phenotypes. *Nature Methods*, 10(9):877–879, 2013. doi: 10.1038/nmeth.2560.
- 589 52 A Vidal-Gadea, S Topper, L Young, A Crisp, L Kressin, E Elbel, and JT Pierce-Shimomura.
590 *Caenorhabditis elegans* selects distinct crawling and swimming gaits via dopamine and
591 serotonin. *Proceedings of the National Academy of Sciences of the United States of America*, 108
592 (42):17504–17509, 2011. doi: 10.1038/nmeth.2560.
- 593 53 VJ Butler, R Branicky, E Yemini, JF Liewald, A Gottschalk, RA Kerr, DB Chklovskii, and
594 WR Schafer. A consistent muscle activation strategy underlies crawling and swimming in
595 *Caenorhabditis elegans*. *Journal of The Royal Society Interface*, 12(102), 2015. doi: 10.1098/rsif.2014.
596 0963.
- 597 54 K Sakata and R Shingai. Neural network model to generate head swing in locomotion of
598 *Caenorhabditis elegans*. *Network*, 15(3):199–216, 2004.
- 599 55 X Deng and JX Xu. A 3d undulatory locomotion model inspired by *C. Elegans* through DNN
600 approach. *Neurocomput.*, 131:248–264, May 2014. ISSN 0925-2312. doi: 10.1016/j.neucom.2013.
601 10.019.
- 602 56 X Deng, JX Xu, J Wang, G Wang, and Q Chen. Biological modeling the undulatory locomotion
603 of *C. elegans* using dynamic neural network approach. *Neurocomputing*, 186:207–217, 2016.
- 604 57 T Xu, J Huo, S Shao, M Po, T Kawano, Y Lu, M Wu, M Zhen, and Q Wen. Descending pathway
605 facilitates undulatory wave propagation in *Caenorhabditis elegans* through gap junctions.
606 *Proceedings of the National Academy of Sciences*, 2018. ISSN 0027-8424. doi: 10.1073/pnas.
607 1717022115.
- 608 58 AD Fouad, S Teng, JR Mark, S Liu, P Alvarez-Illera, H Ji, A Du, PD Bhirgoon, E Cornblath,
609 SA Guan, and C Fang-Yen. Distributed rhythm generators underlie *Caenorhabditis elegans*
610 forward locomotion. *eLife*, 7:e29913, 2018. doi: 10.7554/eLife.29913.